THE JOURNAL OF PHYSICAL CHEMISTRY A LETTERS

2008, *112,* 13275–13281
Published on Web 11/21/2008

310 nm Irradiation of Atmospherically Relevant Concentrated Aqueous Nitrate Solutions: Nitrite Production and Quantum Yields

Maryuri Roca,[†] James Zahardis,[†] Jason Bone,[‡] Mohamed El-Maazawi,[‡] and Vicki H. Grassian*[,†]
Department of Chemistry, University of Iowa, Iowa City, Iowa 52242, and Department of Physical Science and Engineering, Truman College, Chicago, Illinois 60640

Received: October 11, 2008; Revised Manuscript Received: November 8, 2008

The heterogeneous processing of atmospheric aerosols by reaction with nitrogen oxides results in the formation of particulate and adsorbed nitrates. The water content of these hygroscopic nitrate aerosols and consequently the nitrate ion concentration depend on relative humidity, which can impact the physicochemical properties of these aerosols. This report focuses on the 310 nm photolysis of aqueous sodium and calcium nitrate solutions at pH 4 over a wide concentration range of nitrate ion concentrations representative of atmospheric aerosols. In particular, the quantum yield (ϕ) of nitrite formation was measured and found to significantly decrease at high concentrations of nitrate for $Ca(NO_3)_2$. In particular, ϕ for $Ca(NO_3)_2$ was found to have a maximum value of $(7.8 \pm 0.1) \times 10^{-3}$ for nitrate ion solution concentrations near one molal, with the smallest quantum yield for the highest concentration solution above 14 *m* nitrate ion, $\phi = (2.3 \pm 2.0) \times 10^{-4}$. The effect of the addition of the radical scavenger, formate, on the 310 nm photolysis of these solutions was also investigated and found to increase ϕ by a factor of 2 or more for both sodium and calcium nitrate solutions. In the presence of formate, $Ca(NO_3)_2$ solutions again showed a significant decrease in ϕ with increasing NO_3^- concentration: $\phi = (1.4 \pm 0.1) \times 10^{-2}$ at $(1.0 \pm 0.1) \times 10^{-2}$ *m* NO_3^-compared to $\phi = (4.2 \pm 0.3) \times 10^{-3}$ at 14.9 ± 0.1 *m* NO_3^-. This decrease in ϕ was not observed in $NaNO_3$ solutions. The change in electronic structure, as evident by the more pronounced shift of the n$-\pi^*$ absorption band away from actinic wavelengths with increasing concentration for $Ca(NO_3)_2$ compared to $NaNO_3$, is most likely the origin of the greater decrease in ϕ for $Ca(NO_3)_2$ compared to $NaNO_3$ at elevated NO_3^- concentrations. The role of nitrate photochemistry in atmospheric aerosols and the atmospheric implications of these concentration dependent quantum yields are discussed.

Introduction

It is becoming increasing clear that the heterogeneous processing of ubiquitous sea salt and mineral dust aerosol by gas-phase nitrogen oxides (e.g., NO_2, NO_3, N_2O_5, and HNO_3) typically results in the formation of particulate and adsorbed nitrates.[1,2] For example, the NaCl component of sea salt readily reacts with HNO_3 via reaction 1 to yield $NaNO_3$;

$$NaCl(s,aq) + HNO_3(g) \xrightarrow{RH} NaNO_3(s,aq) + HCl(g) \quad (1)$$

The reaction is significantly enhanced at higher relative humidity for the deliquescent salt.[3] Furthermore, heterogeneous reactions with nitrogen oxides convert solid carbonate particulate to aqueous nitrate solutions. In the case of calcite, an important component of desert dust emissions, heterogeneous reactions with gaseous nitric acid occur readily in the atmosphere.[4−6] Above 10% relative humidity (RH), an aqueous calcium nitrate aerosol is formed via the reaction;[7,8]

$$CaCO_3(s) + 2HNO_3(g) \xrightarrow{RH} Ca(NO_3)_2(aq) + CO_2(g) + H_2O \quad (2)$$

Reaction 2 is significant in that the resultant aqueous nitrate aerosol differs in composition, phase, shape, and size compared to the original calcite particle. Moreover, the resultant nitrate aerosol is more hygroscopic and significantly more effective as a cloud condensation nucleus (CCN) than the solid precursor carbonate aerosol.[9,10]

One additional ramification to the formation of nitrate aerosols is that the nitrate ion is photochemically active at solar wavelengths and nitrate photolysis may have an important, albeit poorly understood, role in the further aging of reacted or atmospherically processed sea salt and mineral dust aerosols. It is well-known that photolysis of aqueous nitrate at $\lambda > 290$ nm and pH < 6 proceeds via two main channels:[11−13]

$$NO_3^- + H^+ \xrightarrow{h\nu} NO_2 + OH \quad (3)$$

$$NO_3^- \xrightarrow{h\nu} NO_2^- + O(^3P) \quad (4)$$

The nitrite ion in reaction 3 can undergo further photodissociation ($\lambda_{max} = 354$ nm):

* Author to whom correspondence should be addressed.
[†] University of Iowa.
[‡] Truman College.

10.1021/jp809017b CCC: $40.75

$$NO_2^- + H^+ \xrightarrow{h\nu} NO + OH \quad (5)$$

Hence, nitrate is an active chromophore at actinic wavelengths that is a source of NO_x (i.e., NO + NO_2), as well as a source of OH radicals and $O(^3P)$ as shown in reactions 4 and 5. All of these products represent highly reactive oxidants in both the gas phase as well as in other environmentally relevant phases and at environmentally relevant interfaces, including the surfaces of natural water[14,15] and snowpacks.[16]

Recent ATR-FTIR and UV/vis absorption studies, supported by ab initio calculations, have shown that the molecular and electronic structure of the nitrate ion is a function of the nitrate ion concentration in solution.[17] Although gas-phase NO_3^- is planar and of D_{3h} symmetry, it has been shown that the symmetry of this ion is lowered in the presence of both solvent (e.g., water) molecules and counterions.[17−19] As the NO_3^- symmetry is lowered, the $\pi-\pi^*$ and $n-\pi^*$ transitions become higher in energy, shifting to longer wavelengths. As was shown in the earlier work on aqueous nitrate solutions reported by Hudson et al.,[17] this effect leads to a shift in the UV/vis maximum to longer wavelengths with decreasing NO_3^- concentration. These results strongly suggest that the more concentrated nitrate aerosol, found at lower RH when the water content of the nitrate aerosol is low, will not be as photochemically active in the actinic region of the spectrum (i.e., $\lambda > 290$ nm) compared to the more dilute aerosol when the water content is high.

In addition, recent model calculations by Bauer et al. predict the amount of nitrate in atmospheric particulate matter is likely to increase by the year 2030 as nitrate-precursor emissions increase while sulfate aerosol concentrations simultaneously decrease.[20] Thus suggesting that nitrate aerosols will play an even greater role in atmospheric processes in the future. The current study described herein explores the photochemistry of nitrate solutions, which are used as proxies for aqueous atmospheric aerosols. In particular, the photolysis of aqueous nitrate solutions at 310 nm over a wide range of environmentally relevant concentrations of sodium and calcium nitrate solutions concentrations at pH 4 has been explored. This acidic pH was chosen as it has been suggested that once the carbonate is titrated, additional nitric acid uptake by atmospheric aerosols results in low pH environments.[21] The quantum yield of one of the main products of nitrate photolysis, the nitrite ion, is correlated with the change in the electronic structure of the nitrate ion as observed by an actinic shift in the absorption band of the irradiated solutions that occurs with increasing dilution. The effect of formate, an OH scavenger, on the photolysis of nitrate solutions production is investigated. The implications arising from the photochemistry of aqueous nitrate aerosols as these aerosols are transported through the atmosphere are discussed.

Experimental Methods

Source of Chemicals and Solution Preparation. Calcium nitrate tetrahydrate (Alfa Aesar, ACS grade), sodium nitrate (Alfa Aesar, ACS grade), sodium nitrite (Alfa Aesar, ACS grade) and sodium formate (Sigma, ACS grade) were used without further purification. The potassium ferrioxalate actinometer was prepared by the method of Hatchard and Parker,[22] from potassium trioxalatoferrate(III) trihydrate ($K_3Fe(C_2O_4)_3 \cdot 3H_2O$, Alfa Aesar) and sulfuric acid (Mallinckrodt, 100%). Griess reagent, which was used for the colorimetric quantification of nitrite, was obtained from Alexis Biochemicals (#ALX-400-004-L050). All solutions were prepared with Optima water (Fisher Chemical). Sodium and calcium nitrate solutions were prepared with similar concentrations of the nitrate ion, from ca. 0.01−6 *m*. Higher concentrations of the $NaNO_3$ solutions could not be assayed because crystals of the salt were observed at elevated concentrations. An upper limit for the calcium nitrate salt were determined to be near 15 *m* nitrate ion concentration since no crystals were observed for this solution, although at this concentration it may be best described as a glassy solution.[23−25]

UV/Vis Spectroscopy. The UV/vis measurements employed a Lambda 20 UV/vis spectrophotometer (Perkin-Elmer Instruments) to measure the absorption maximum of the $n-\pi^*$ transition. UV/vis quartz cuvettes, with pathlengths of 1 cm (Light Path Cells, Inc.), 1 mm (NSG Precision Cells, Inc.), and 0.1 mm (Perkin-Elmer Instruments) were used to acquire absorption spectra over a large concentration range. Disposable 1 cm path length cuvettes (Fisher Scientific) were employed for all colorimetric determinations.

Photolysis of Nitrate Solutions: Quantum Yield Determination. Aqueous calcium and sodium nitrate solutions were prepared with and without 10 mM sodium formate, which acted as a radical scavenger. All solutions were adjusted to pH 4 prior to irradiation. Irradiation was carried out in a cylindrical glass cell (3.5 cm i.d., 13.5 cm height), and all photolysis reactions were carried out under isothermal conditions (298 ± 1 K) by use of a water jacket; with the solutions constantly stirred with a small magnetic stir bar. The optical path length employed was 1 cm, with an overhead 500 W mercury lamp (Oriel Corporation) as the light source, employing a water cooled near-IR filter (Oriel) and a 310 ± 10 nm band-pass filter (Asahi Spectra).

Samples were irradiated for up to 15 min, with colorimetric measurements taken on aliquots every five minutes to determine the rate of formation of the nitrite ion. The nitrite produced was determined colorimetrically using Greiss reagent, a well established protocol.[26] In aqueous media at 298 K reaction 3, which forms nitrogen dioxide, usually has a quantum yield of over order of magnitude greater than reaction 4, which forms the nitrite ion.[27−29] As will be discussed, in the cases where the radical scavenger formate is added to the solution, the nitrite ion will be the predominant reaction product of the photolysis of nitrate. We will compare the rate of nitrite formation and the quantum yields for nitrate solutions with and without formate.

The quantum yield for the photolysis of aqueous nitrate solutions at 310 nm, can be calculated via the following equation:[28]

$$\phi = \frac{\text{Rate}(NO_2^-)V}{I_o(1 - e^{-2.303\varepsilon m l})} \quad (6)$$

where Rate(NO_2^-) is the moles per liter of NO_2^- produced per minute, V is the volume of the irradiated solution (liters), I_o is the light intensity (E min^{-1}), ε (m^{-1} cm^{-1}) is the extinction coefficient for the photolysis of nitrate at 310 nm, m is the molality (mol kg^{-1}) of nitrate in the irradiated solution, and l denotes the path length of the irradiated solution (1 cm).

The light intensity, I_o, was determined via actinometry with potassium ferrioxalate. The extinction coefficient, ϵ, was determined for each of the nitrate solutions (Figure 1). It should be noted that the concentration of the nitrate ion is given in units of molality (m), and subsequently the extinction coefficient will be expressed in units of m^{-1} cm^{-1}. Because the calcium

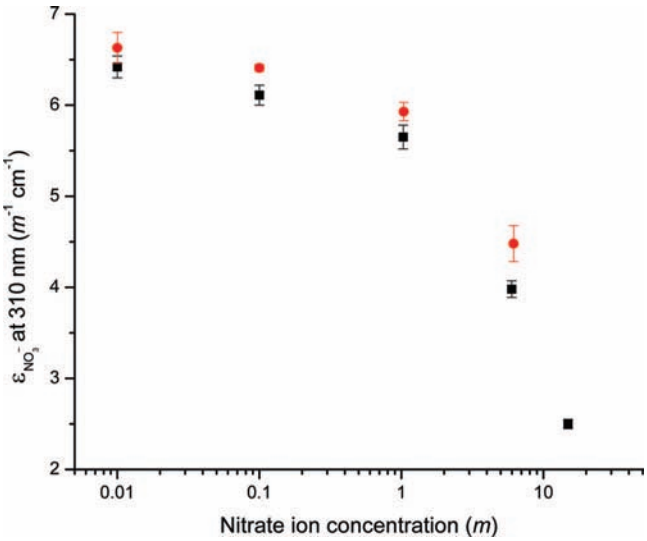

Figure 1. Extinction coefficient of aqueous solutions of the nitrate ion at 310 nm. ■ and ●, respectively, denote nitrate solutions derived from $Ca(NO_3)_2$ and $NaNO_3$.

nitrate solutions employed will be extended to concentrations where transitions to glass-like solutions[23−25] occurs, these solutions will likely exhibit nonideal solution behavior. As given in Hudson et al., the molarity of nitrate can be calculated from the molality of the solution.[17]

Reported errors for solution concentrations have been determined from the propagation error associated with the accuracy of the volumetric and mass measurements needed to prepare the solution. For nitrite production at a given concentration, the error in each data point is reported here from the standard deviation of at least three measurements. Initial rate data use a linear regression analysis of the slope of the data. The error in the quantum yield was determined using the propagation of the errors discussed above as well as errors in the measured light flux and epsilon determined from the standard deviation of triplicate measurements.

Results and Discussion

Photolysis of Calcium and Sodium Nitrate Aqueous Solutions. There are often real limitations to Beer's law in concentrated solutions of electrolytes, such as the nitrate solutions investigated in the studies reported herein; hence, as shown in Figure 1, the extinction coefficient (ε) was calculated across the range of concentrations employed. For both calcium and sodium nitrate solutions, the extinction coefficient was found to depend on the concentration of nitrate ion especially above one molal, demonstrating the nonideality of these highly concentrated solutions. As seen in Figure 1, there is a monotonic decrease in ε with increasing concentration. The range of the extinction coefficient for calcium nitrate solutions was from 2.5 $\pm$ 0.1 to 6.4 $\pm$ 0.1 m^{-1} cm^{-1}, for respective concentrations from 14.9 $\pm$ 0.1 m to (1.1 $\pm$ 0.1) $\times$ 10^{-2} m NO_3^-. The decrease in the extinction coefficient with increasing nitrate concentration is in accord with the previous work reported by Hudson et al.[17] that showed a decrease in the extinction coefficient at 301 nm, for calcium nitrate solutions from ca. 0.16−30.8 m NO_3^- with ε ranging from ca. 2.0 to 6.4 m^{-1} cm^{-1}. In the current study, for aqueous sodium nitrate solutions, the extinction coefficient was from 4.5 $\pm$ 0.2 to 6.6 $\pm$ 0.2 m^{-1} cm^{-1}, for respective concentrations from 6.2 $\pm$ 0.1 m to (1.1 $\pm$ 0.1) $\times$ 10^{-2} m NO_3^-. For the sodium nitrate solutions, the extinction coefficient determined at 310 nm at the lower concentration limit, ε = 6.6 $\pm$ 0.2 m^{-1} cm^{-1}, is in excellent agreement with the value of ϵ reported by others at similar concentrations.[12,30]

The quantum yield (ϕ) for the 310 nm irradiated aqueous nitrate solutions was determined via (eq 6), using the appropriate extinction coefficient (vide supra). The light intensity, I_o, was determined to be (2.3 $\pm$ 0.2) $\times$ 10^{-7} E min^{-1} using the potassium ferrioxalate actinometer. The quantum yield is directly proportional to the rate of nitrite formation (eq 6). Parts a and c of Figure 2 compare the rate of nitrite formation, for the sodium and calcium nitrate solutions, respectively. As shown in Figure 2a, for sodium nitrate solutions, the photolytic rate increases for the three lower nitrate concentration solutions from (2.1 $\pm$ 0.3) $\times$ 10^{-2} to (2.1 $\pm$ 0.2) $\times$ 10^{-1} μM min^{-1} for solutions with concentrations ranging from (1.0 $\pm$ 0.1) $\times$ 10^{-2} to 1.1 $\pm$ 0.1 m. However, the rate of nitrite formation is reversed for the two highest concentration solutions: with the 6.2 $\pm$ 0.1 m solution rate of nitrite formation decreasing to (8 $\pm$ 2) $\times$ 10^{-2} μM min^{-1}. As shown in Figure 2b, the quantum yield consequently increases from 4.5 $\times$ 10^{-3} to 6.3 $\times$ 10^{-3} for (1.0 $\pm$ 0.1) $\times$ 10^{-2} to 1.0 $\pm$ 0.1 m solutions but decreases to 2.5 $\times$ 10^{-3} for the most concentrated solution of 6.2 $\pm$ 0.1 m NO_3^-. As will be explained, this photochemical feature most likely arises from the shift in the band maximum of the wavelength of absorption to a shorter wavelength for the highly concentrated sodium nitrate solution.

The quantum yield for calcium nitrate solutions was determined in a similar manner as for the sodium nitrate solutions. Parts c and d of Figure 2 show the key results for the calcium nitrate derived solutions. For the three lower concentration solutions the rate of photolysis increases from (2.7 $\pm$ 0.8) $\times$ 10^{-2} to (2.6 $\pm$ 0.2) $\times$ 10^{-1} μM min^{-1} for solutions from (1.0 $\pm$ 0.1) $\times$ 10^{-2} to 1.0 $\pm$ 0.1 m NO_3^-. However, as shown in Figure 2c, the rate of photolysis decreases for the latter three concentrations, to (8 $\pm$ 6) $\times$ 10^{-3} μM min^{-1} for the solution 14.9 $\pm$ 0.1 m NO_3^-. Similarly, the quantum yield, ϕ, reaches the maximum value of (7.8 $\pm$ 0.1) $\times$ 10^{-3} for the 1.03 $\pm$ 0.01 m solution, with a significantly diminished quantum yield at 14.9 $\pm$ 0.1 m, with ϕ = (2.3 $\pm$ 2.0) $\times$ 10^{-4}. This is notable in that the *lowest quantum yield* corresponds to the calcium nitrate solution with the *highest nitrate ion concentration*.

Photolysis of Calcium and Sodium Nitrate Aqueous Solutions with Formate. The effects of a radical scavenger on the rate of photolysis at 310 nm and quantum yield were investigated. Formate (HCO_2^-) was utilized as the radical scavenger because it has well-established reactivity with the hydroxyl radical:[31]

$$HCO_2^- + OH \rightarrow H_2O + CO_2^- \quad (7)$$

The addition of this radical scavenger to the nitrate solutions prevents NO_2^- loss by consuming hydroxyl radicals that react with the nitrite ion forming NO_2:[31]

$$NO_2^- + OH \rightarrow NO_2 + OH^- \quad (8)$$

Also, as shown by Dubowski et al.,[31] the nitrogen dioxide, which is the major product of photolysis sans formate, is converted to nitrite by reactions 9−11 with in situ generated superoxide (O_2^-):

$$HCO_2^- + OH \rightarrow H_2O + CO_2^- \quad (9)$$

$$CO_2^- + O_2 \rightarrow O_2^- + CO_2 \quad (10)$$

$$O_2^- + NO_2 \rightarrow O_2 + NO_2^- \quad (11)$$

As shown in Figure 3a, for sodium nitrate solutions with formate, the photolysis rate increases with the concentration of the nitrate ion, from $(3.7 \pm 0.2) \times 10^{-2}$ to $(4.1 \pm 0.1) \times 10^{-1}$ μM min^{-1} for solutions ranging from $(1.0 \pm 0.1) \times 10^{-2}$ to 6.2 $\pm$ 0.1 *m*. In addition, the quantum yield is greater for all sodium nitrate solutions containing the radical scavenger (cf. Figures 2b and 3b); with the most significant difference a factor of ~5 for the most concentrated solution (at 6.2 $\pm$ 0.1 *m* $NaNO_3$). This is in accord with a similar increase determined by Dubowski et al.[31] This increase in the quantum yield is in accord with the net increase in the nitrite ion due to the scavenging of OH by formate, which is a sink for nitrite (reaction 8). The quantum yields were calculated in a manner identical to described previously: as shown in Figure 3b, the lowest value of the quantum yield was $(7.9 \pm 0.8) \times 10^{-3}$, which was determined from the solution with the lowest initial concentration of nitrate of $(1.1 \pm 0.1) \times 10^{-2}$ *m* NO_3^-. The highest quantum yield was $(1.3 \pm 0.6) \times 10^{-2}$, which was determined for the highest concentration of nitrate solution (6.2 $\pm$ 0.1 *m*).

The quantum yields determined for $NaNO_3$ are in good agreement with previous studies at similar wavelengths, although to the best of our knowledge this is the first extensive study of aqueous solutions of sodium nitrate at 310 nm. Goldstein and Rabani[32] determined $\phi_{NO_2^-}$ at 300 nm to be $(9.4 \pm 0.2) \times 10^{-3}$, for 0.02−1 M sodium nitrate solutions with formate (pH 4.2 −4.5), which is in good agreement for aqueous solutions of sodium nitrate and formate, which have a quantum yield of ca. (7.9−9.4) $\times$ 10^{-3} at pH 4 across this concentration range. Similarly, Warneck and Wurzinger[27] investigated the 305 nm photodecomposition of nitrate solutions and determined that for 0.01 M $NaNO_3$ solutions with formate (pH 5.6) $\phi_{NO_2^-}$ = (8.4−9.7) $\times$ 10^{-3}. The small difference between our value of the quantum yield at this concentration of $NaNO_3$ and that of Warneck and Wurzinger likely arises from the differences in the pH of the solution (pH 4 vs 5.6) and the differences in the irradiation wavelength (310 vs 305 nm). Dubowski et al.[31] have studied the temperature dependence of the quantum yield of 313 nm irradiated solutions of sodium nitrate with and without the presence of formate; however, these studies went to a maximum temperature of 294 K, compared to the current study at 298 K. By extrapolation, they estimate that for solutions of $NaNO_3$ with formate (1 mM $NaNO_3$/10 mM $NaCO_2H$) that $\phi_{NO_2^-} \sim 0.02$ at 298 K. This is over a factor of 2 greater than the quantum yield for our lowest concentration solution, which was 1 order of magnitude more concentrated in nitrate than the solutions investigated by Dubowski et al.[31] Similarly, for $NaNO_3$ solutions without the radical scavenger, with comparable

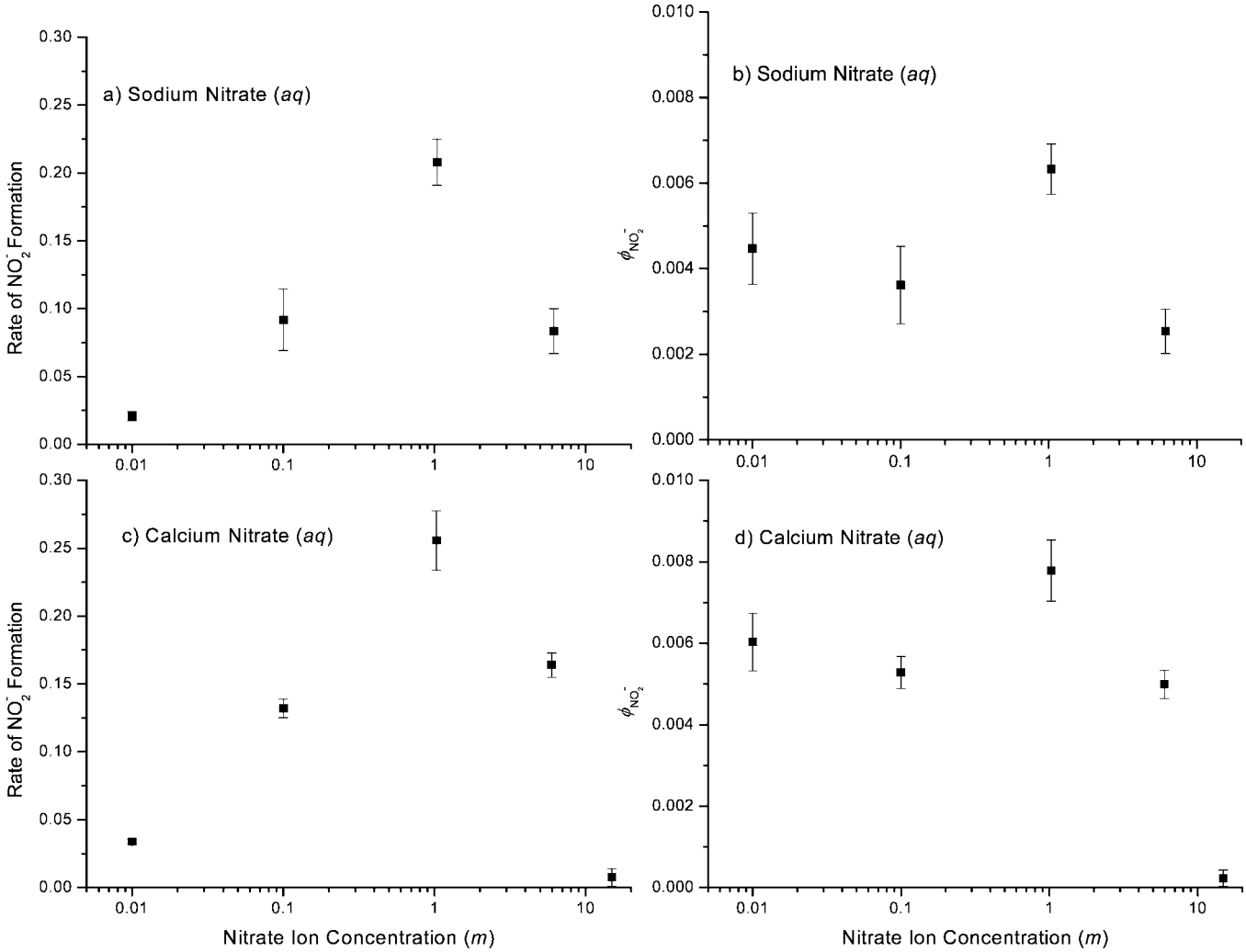

Figure 2. (a) Rate of nitrite ion formation (μM min^{-1}) and (b) quantum yield ($\phi_{NO_2^-}$) for $NaNO_3$ solutions. (c) Rate of nitrite ion formation (μM min^{-1}) and (d) and quantum yield of nitrite ion formation for $Ca(NO_3)_2$ solutions. The wavelength of photolysis was 310 $\pm$ 10 nm and all solutions were prepared without the radical scavenger, formate.

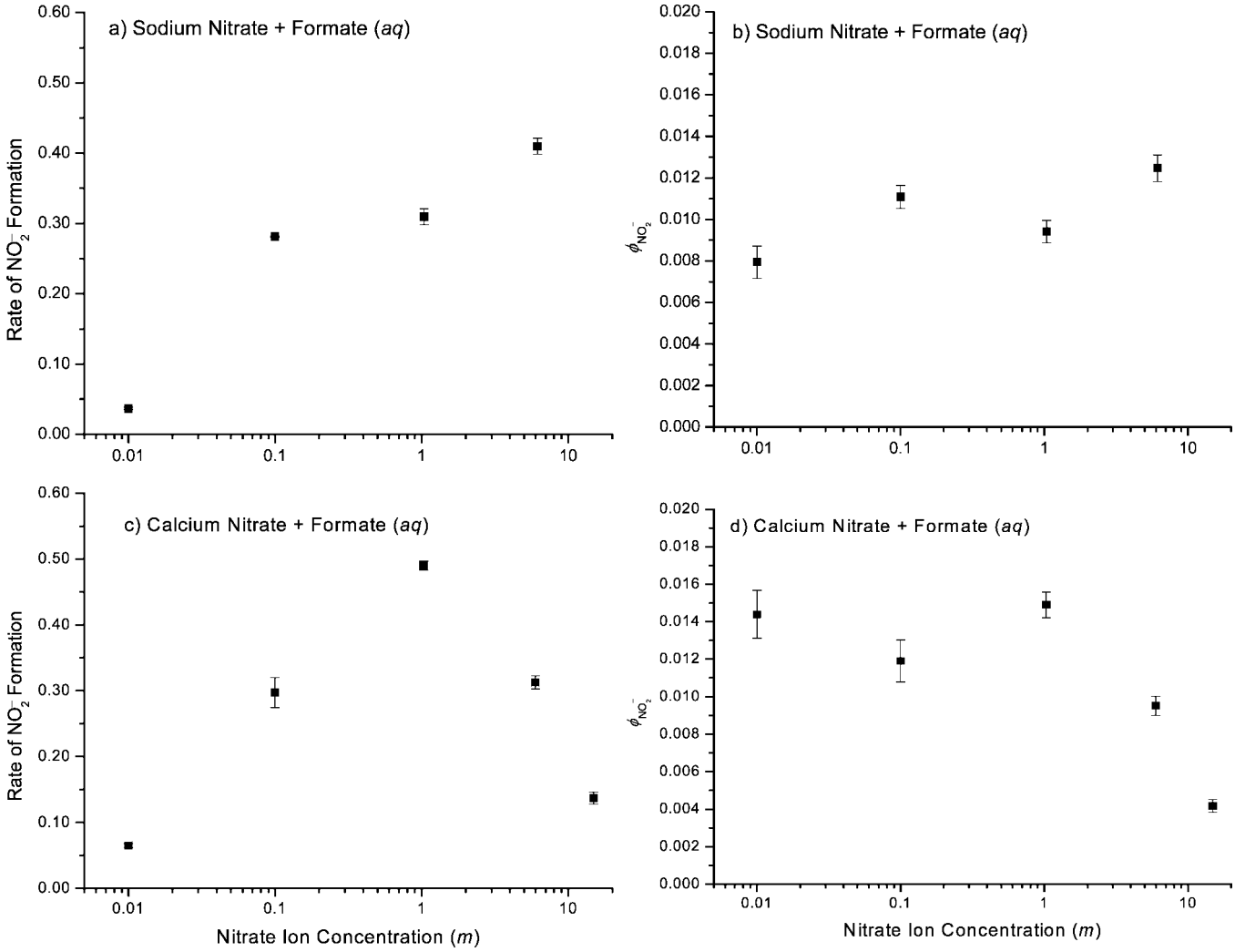

Figure 3. (a) Rate of nitrite ion formation (μM min^{-1}) and (b) quantum yield ($\phi_{NO_2^-}$) for $NaNO_3$ solutions. (c) Rate of nitrite formation (μM min^{-1}) and (d) quantum yield ($\phi_{NO_2^-}$) for $Ca(NO_3)_2$ solutions. The wavelength of photolysis was 310 ± 10 nm and all solutions were prepared with the radical scavenger, formate.

concentrations of nitrate (i.e., on the order of 0.1 M), the quantum yield measured here is about a factor of 2 smaller than that of Dubowski et al. (ca. 4×10^{-3} vs 8×10^{-3}), with the latter value our estimate of the quantum yield from Dubowski et al. (Figure 6 in ref 31). The differences in quantum yields between these studies most likely arise from the differences in the irradiation wavelengths as well as pH, the latter of which has been indicated as a significant factor in formation of nitrite by photodecomposition of nitrate.[12,27] This pH dependence on nitrite formation may arise from the equilibrium between peroxynitrous acid (HOONO) and its conjugate base, the peroxynitrite anion ($ONOO^-$), which has been indicated to be the main product of photolysis of nitrate[32,33] and suggests that the products given by reactions 3 and 4 are from reactions occurring in the photolyzed solution over time. Although the mechanistic details of the formation of nitrite are not the focus of this report, and are covered in detail elsewhere,[12,32,33] the complexity of the photodynamics of nitrate photolysis is noted because it strongly suggests that *both* the wavelength of irradiation and pH must be considered when comparing the quantum yield of nitrate solutions from different studies.

Figure 3c depicts the rate of photolysis for calcium nitrate solutions, in the presence of formate, which by comparison to Figure 2c shows a factor of ca. 2 increase in the rate of photolysis when formate is added to the solution. The photolytic rate increases with initial nitrate concentration, from $(6.5 \pm 0.3) \times 10^{-2}$ to a maximum rate of $(4.9 \pm 0.1) \times 10^{-1}$ μM min^{-1} for solutions from $(1.1 \pm 0.1) \times 10^{-2}$ to 1.1 ± 0.1 *m*. This is followed by a significant decrease in the rate of photolysis with the most concentrated nitrate solution (14.9 ± 0.1 *m*) having a rate of $(1.4 \pm 0.10) \times 10^{-1}$ μM min^{-1}. Figure 3d depicts the quantum yield of calcium nitrate solutions containing the radical scavenger, formate. The quantum yield of the most dilute solution of $(1.0 \pm 0.1) \times 10^{-2}$ *m* NO_3^- is $(1.4 \pm 0.1) \times 10^{-2}$ that is over a factor of 3 times greater than ϕ for the most concentrated solution of $(4.2 \pm 0.3) \times 10^{-3}$ at 14.9 ± 0.1 *m* NO_3^-, which is the minimum quantum yield for the calcium nitrate solutions assayed. To the best of our knowledge these are the only determinations of the quantum yield for calcium nitrate solutions at 310 nm or similar wavelengths.

UV/Vis Spectroscopy of Nitrate Solutions. The band maximum in the spectral region for the n−π* transition of $Ca(NO_3)_2$ and $NaNO_3$ solutions was investigated by UV/vis absorption spectroscopy. The changes in the UV/vis optical properties of concentrated nitrate solutions have been described in an earlier report;[17] hence the following discussion focuses on the shift of the n−π* band maxima toward longer wavelengths with increasing dilution and the corresponding changes in the quantum yield at 310 nm.

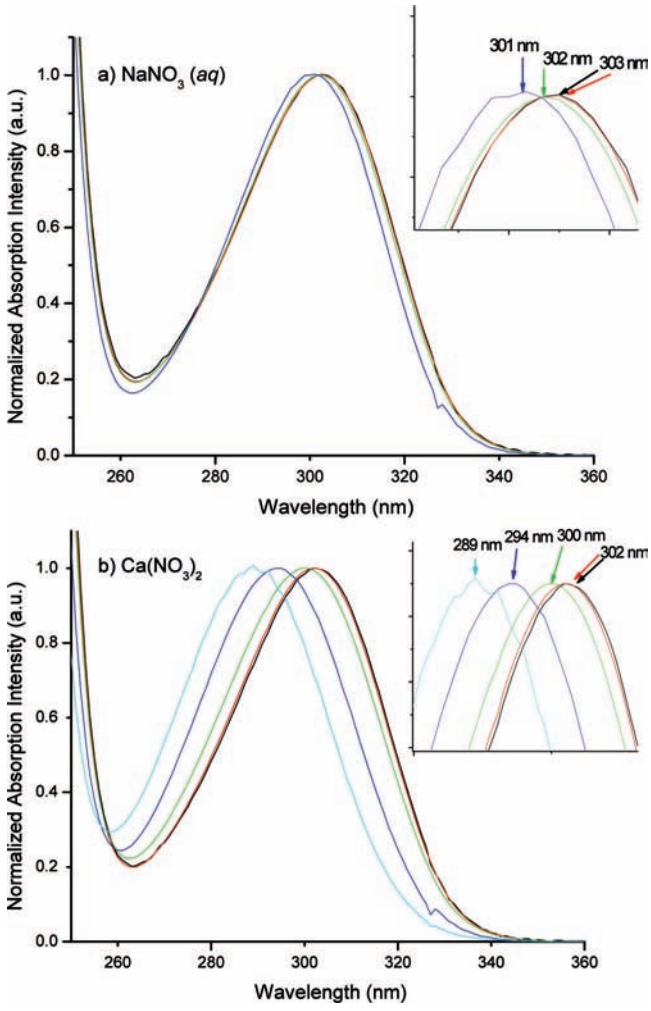

Figure 4. Normalized intensity of UV/vis absorption for nitrate solutions from (a) $NaNO_3$ [color key: (black), (red), (green) and (blue) denote 0.01, 0.1, 1.0, and 6.2 *m* NO_3^- solutions] (b) solutions from $Ca(NO_3)_2$ [color key: (black), (red), (green), (blue), and (light blue) denote 0.01, 0.1, 1.0, 6.0 and 14.9 *m* NO_3^- solutions]. Insets highlight the shifts in the band maximum for $NaNO_3$ and $Ca(NO_3)_2$. All absorption spectra normalized to unit intensity.

Parts a and b of Figure 4 compare the shift in the band maximum for calcium and sodium nitrate solutions, showing a much more significant shift toward the actinic region of the spectrum for calcium nitrate solutions. For sodium nitrate solutions there is only a 2 nm shift in the band maximum absorption for the n$-\pi^*$ transition, from 301 to 303 nm, respectively for 6.2 ± 0.1 *m* to $(1.0 \pm 0.1) \times 10^{-2}$ *m* NO_3^- solutions. However, the shift toward longer wavelengths with increasing dilution for calcium nitrate solutions is far more significant: there was a monotonic increase in the band maximum from 289 to 302 nm, respectively, for solutions that ranged from 14.9 ± 0.1 *m* to $(1.0 \pm 0.1) \times 10^{-2}$ *m* NO_3^-. This shift is more pronounced at high concentrations: for the concentration range 1.0$-$0.1 *m* the maximum only increases by 2 nm (from 300 to 302 nm); conversely from 14.9 ± 0.1 to 1.0 ± 0.1 *m* NO_3^- the shift is 11 nm (from 289 to 300 nm). Succinctly, the shift of the band maximum to longer wavelength with increasing dilution is more pronounced with calcium nitrate than sodium nitrate solutions, indicating a change in the electronic structure of nitrate in these concentrated divalent ionic solutions which leads to a a decrease in quantum yields for the photolysis of the $Ca(NO_3)_3$ solutions at high concentrations of nitrates, which is not evident in the sodium nitrate solution.

Conclusions and Atmospheric Implications

We have correlated the photolytic and UV/vis spectroscopic properties of two atmospherically relevant aqueous nitrate solutions, $NaNO_3$ and $Ca(NO_3)_2$. We have shown the n$-\pi^*$ band maximum shifts toward actinic wavelengths with increasing dilution, with a much more pronounced effect for $Ca(NO_3)_2$ than $NaNO_3$ based solutions. This effect is in accord with results presented by Hudson et al.[17] at 301 nm with $Ca(NO_3)_2$ solutions; with molecular symmetry based arguments for these observations presented in that report. The current study shows how these changes in electronic structure impacts the quantum yield of photolysis: for the calcium nitrate solutions there is a pronounced decrease in quantum yield of nitrite at high nitrate concentrations, for solutions with and without the radical scavenger, formate (cf. Figures 3d and 2d). This effect is not evident or as pronounced for $NaNO_3$, respectively with and without formate, at the highest concentrations of nitrate (6.16 *m*). It should be noted that the most significant decrease in the quantum yield for 310 nm photolysis of nitrate was for nitrate solutions near fifteen molal that were only assayed with $Ca(NO_3)_2$, since $NaNO_3$ formed crystals at this concentration, which were not observed in the former salt. This does *not* imply that the solutions of $Ca(NO_3)_2$ were ideal; calcium nitrate is noted as being an extremely "fragile" solution,[25] which is characterized by having very broad glass transition width. The nearly constant ratio of the glass transition temperature for calcium nitrate, T_g to T_o (from the Vogel$-$Fulcher$-$Tamman equation; see Angell[25] for details) implies that this fragility is constant for *all* compositions of calcium nitrate. It is very likely that our solutions of $Ca(NO_3)_2$ underwent liquid structural transitions in the concentration range employed because aqueous calcium nitrate below 6% (mole percent in calcium nitrate, cf. the highest concentration nitrate solution in this study, which is ca. 12% mol $Ca(NO_3)_2$) at room temperature have a transition from a highly structured to less structures liquid transition.[23,25] This concentration dependent liquid structural transition along with the changes in the molecular symmetry of the nitrate ion[17] may contribute to the pronounced deviation from Beer's law in the absorption at 310 nm as given by the concentration dependence of the extinction coefficient (Figure 1).

The pronounced blue shift to shorter wavelengths for the n$-\pi^*$ band maximum (Figure 4b) with increasing nitrate ion concentration has significant atmospheric implications. The exposure of ubiquitous calcite particulate matter to nitrogen oxides in the polluted troposphere may result in a quantitative conversion to $Ca(NO_3)_2$,[4$-$6] which is highly hygroscopic. The conversion of calcite to $Ca(NO_3)_2$ and the formation of surface adsorbed nitrate may lead to interesting heterogeneous photochemistry including an RH dependent source of NO_x (NO + NO_2), important photochemically derived oxidants, as well as N_2O, a greenhouse gas.[34] The formation of photooxidants that may arise from the photolysis of nitrate has been very recently shown by Finlayson-Pitts and co-workers to have important implications on the oxidation of organic species ubiquitous to environmentally relevant interfaces.[35,36] The current study has shown that nitrite forms in the solution phase. It can be further speculated that NO_2 can go into the gas phase at the aerosol interface, contributing to NO_x,[37] and the photolysis yield of NO_2 formation at the interface may vary by over an order of magnitude as a function of RH due to the variation in nitrate ion concentration with RH. Furthermore, the exact nature of the surface of aqueous nitrate aerosols is complex and very recent experimental[38] and theoretical studies[39$-$41] suggest that the surface differs in nature to the bulk liquid and, in turn, imply

that photochemical processes at the surface of the aqueous aerosol may differ from the bulk. Thus, it is important in future studies to investigate the photolysis of aqueous calcium nitrate aerosols directly as well as investigate the photochemical properties of multicomponent proxy solutions and aerosol that more accurately reflect the composition of actual aqueous atmospheric aerosol. These studies should be done over a wide range of nitrate concentrations where deviations from ideal solution behavior may exist and impact photochemical reactions of atmospheric relevance.

Acknowledgment. This work reported herein was funded by the NSF under grant CHE503854. Any opinions, findings and conclusions or recommendations expressed in this material are those of the authors and do not reflect the views of the NSF. J.B. was supported in part by the City Colleges of Chicago through an Undergraduate Research Collaborative grant.

References and Notes

(1) Finlayson-Pitts, B. J.; Hemminger, J. C. *J. Phys. Chem. A* **2000**, *104*, 11463–11477.
(2) Grassian, V. H. *Int. Rev. Phys. Chem.* **2001**, *20*, 467–548.
(3) ten Brink, H. *J. Aerosol Sci.* **1998**, *29*, 57–64.
(4) Laskin, A.; Iedema, M. J.; Ichkovich, A.; Graber, E. R.; Taraniu, I.; Rudich, Y. *Faraday Discuss.* **2005**, *130*, 453–468.
(5) R. C. Sullivan, R. C.; Guazzotti, S. A.; Sodeman, D. A.; Prather, K. A. *Atmos. Chem. Phys* **2007**, *7*, 1213–1236.
(6) Shia, Z.; Daizhou Zhang, D.; Hayashi, M.; Ogatab, H.; Ji, H.; Fujiie, W. *Atmos. Environ.* **2008**, *42*, 822–827.
(7) Liu, Y.; Gibson, E. R.; Cain, J. P.; Wang, H.; Grassian, V. H.; Laskin, A. *J. Phys. Chem. A* **2008**, *112*, 1561–1571.
(8) Preszler Prince, A.; Grassian, V. H.; Kleiber, P.; Young, M. A. *Phys. Chem. Chem. Phys.* **2007**, *9*, 622–634.
(9) Gibson, E. R.; Hudson, P. K.; Grassian, V. H. *Geophys. Res. Lett.* **2006**, *33*, L13811.
(10) Kelly, J. T.; Chuang, C. C.; Wexler, A. S. *Atmos. Environ.* **2007**, *41*, 2904–2916.
(11) Dubowski, Y.; Colussi, A. J.; Hoffmann, M. R. *J. Phys. Chem. A* **2001**, *105*, 4928–4932.
(12) Mack, J.; Bolton, J. R. *J. Photochem. Photobiol. A* **1999**, *128*, 1–13.
(13) Mark, G.; Korth, H.-G.; Schuchmann, H.-P.; von Sonntag, C. *J. Photochem. Photobiol. A* **1996**, *101*, 89–103.
(14) Acker, K.; Beysens, D.; Möller, D. *Atmos. Res.* **2008**, *87*, 200–212.
(15) Young, M. A. *Environmental Photochemistry in Surface Waters*; John Wiley & Sons: New York, 2005.
(16) Grannas, A. M.; Jones, A. E.; Dibb, J.; Ammann, M.; Anastasio, C.; Beine, H. J.; Bergin, M.; Bottenheim, J. W.; Boxe, C. S.; Carver, G.; Chen, G.; Crawford, J. H.; Dominé, F.; Frey, M. M.; Guzmán, M. I.; Heard, D. E.; Helmig, D.; Hoffmann, M. R.; Honrath, R. E.; Huey, L. G.; Hutterli, M.; Jacobi, H. W.; Klán, P.; Lefer, B.; McConnell, J.; Plane, J.; Sander, R.; Savarino, J.; Shepson, P. B.; Simpson, W. R.; Sodeau, J. R.; von Glasow, R.; Weller, R.; Wolff, E. W.; Zhu, T. *Atmos. Chem. Phys.* **2007**, *7*, 4329–4373.
(17) Hudson, C. E.; Schwarz, J.; Baltrusaitis, J.; Gibson, E. R.; Grassian, V. H. *J. Phys. Chem. A* **2007**, *111*, 544–548.
(18) Waterland, M. R.; Stockwell, D.; Kelley, A. M. *J. Chem. Phys.* **2001**, *114*, 6249–6258.
(19) Zhang, Y.-H.; Choi, M. Y.; Chan, C. K. *J. Phys. Chem. A* **2004**, *108*, 1712–1718.
(20) Bauer, S. E.; Koch, D.; Unger, N.; Metzger, S. M.; Shindell, D. T.; Streets, D. G. *Atmos. Chem. Phys.* **2007**, *7*, 5043–5059.
(21) Meskhidze, N.; Chameides, W. L.; Nenes, A. *J. Geophys. Res.* **2005**, *110*, DO3301.
(22) Hatchard, C. G.; Parker, C. A. *Proc. R. Soc. London A* **1956**, *235*, 518–536.
(23) Angell, C. A.; Bressel, R. D. *J. Phys. Chem.* **1972**, *76*, 3244–3253.
(24) Fleissner, G.; Hallbrucker, A.; Mayer, E. *J. Phys. Chem.* **1993**, *97*, 4806–4814.
(25) Angell, C. A. *Chem. Rev.* **2002**, *102*, 2627–2650.
(26) Huygen, I. C. *Anal. Chem.* **1970**, *42*, 407–409.
(27) Warneck, P.; Wurzinger, C. *J. Phys. Chem.* **1988**, *92* (22), 6278–6283.
(28) Zellner, R.; Exner, M.; Herrmann, H. *J. Atmos. Chem.* **1990**, *10*, 411–425.
(29) Calvert, J. G.; Pitts, J. N., Jr. *Photochemistry*; John Wiley & Sons, Inc.: New York, 1966.
(30) Chu, L.; Anastasio, C. *J. Phys. Chem. A* **2003**, *107*, 9594–9602.
(31) Dubowski, Y.; Colussi, A. J.; Boxe, C.; Hoffmann, M. R. *J. Phys. Chem. A* **2002**, *106*, 6967–6971.
(32) Goldstein, S.; Rabani, J. *J. Am. Chem. Soc.* **2007**, *129*, 10597–10601.
(33) Madsen, D.; Larsen, J.; Jensen, S. K.; Keiding, S. R.; Thøgersen, J., T. *J. Am. Chem. Soc.* **2003**, *125*, 15571–15576.
(34) Schuttlefield, J.; Rubasinghege, G.; El-Maazawi, M.; Bone, J.; Grassian, V. H. *J. Am. Chem. Soc.* **2008**, *130*, 12210–12211.
(35) Yu, Y.; Ezell, M. J.; Zelenyuk, A.; Imre, D.; Alexander, L.; Ortega, J.; Thomas, J. L.; Gogna, K.; Tobias, D. J.; D'Anna, B.; Harmon, C. W.; Johnson, S. N.; Finlayson-Pitts, B. J. *Phys. Chem. Chem. Phys.* **2008**, *10*, 3063–3071.
(36) Karagulian, F.; Dilbeck, D. W.; Finlayson-Pitts, B. J. *J. Am. Chem. Soc.* **2008**, *130*, 11272–11273.
(37) Handley, S. R.; Clifford, D.; Donaldson, D. J. *Environ. Sci. Technol.* **2007**, *41*, 3898.
(38) Shamay, E. S.; Buch, V.; Parrinello, M.; Richmond, G. L. *J. Am. Chem. Soc.* **2007**, *129*, 12910–12911.
(39) Thomas, J. L.; Roeselova, M.; Dang, L. X.; Tobias, D. J. *J. Phys. Chem. A* **2007**, *111*, 3091–3098.
(40) Bianco, R.; Wang, S. Z.; Hynes, J. T. *J. Phys. Chem. A* **2008**, *112*, 9467–9476.
(41) Bianco, R.; Wang, S.; Hynes, J. T. Advances in Quantum Chemistry: Applications of Theoretical Methods to Atmospheric Science. In *Adv. Quantum Chem.* **2008**, *55*, 387−405.

JP809017B